Asian Journal of Atmospheric Environment

RESEARCH ARTICLE Open Access

A comparative study of the UV index between OMI and ground-based measurements in Nepal

Umakant L. Karna[1,2*], Khem N. Poudyal[3†], Babu R. Tiwari[3†] and Binod K. Bhattarai[3†]

Abstract

The study on solar ultraviolet radiation (UVR) is essential for understanding the solar status of any location, which enables the determination of the level of exposure to solar UV radiation and the necessary precautions to be taken at that location. The measurement of solar UV radiation and its validation are increasingly prevalent worldwide, using various ground-based observations and satellite estimates. This paper compares the Ozone Monitoring Instrument (OMI)/Aura satellite solar ultraviolet index (UVI) with the ground-based UVI measurements at Biratnagar, Pokhara, Kathmandu, and Lukla in Nepal using data from 2009 to 2012. Trend analysis of UVI using moving averages, a box plot of overpass UVI and Total Ozone Column (TOC) to analyze their trends, and a scatter plot for comparison of OMI overpass UVI with ground-based UVI. Statistical tools were used to compare the datasets for UVI in all-sky conditions. The results show that satellite estimates tended to overestimate ground-based UVI levels, with a mean bias, relative bias, MAPE, RMSE, correlation coefficient, and standard deviation of error corresponding to 0.92, 1.9, 28.44, 1.6, 0.69, and 1.44 for UVI, respectively. The result also shows that the altitude effect is found to be (6.5-8.8) %/km approximately.

Keywords Ground-based measurements, Statistical tools, OMI, TOC, UVI

1 Introduction

Nepal, a landlocked country, lies between latitudes 26° 22' N and 30° 27' N and longitudes 80° 40' E and 88° 12'. Its altitude ranges from lowland (60 m) to the High Himalayan peaks, including Mt. Everest (8848.86 m), surrounded by India and China. The country extends approximately 800 km in length and 200 km in width, covering an area of 1,47,516 km^2 (Adhikari et al., 2013; Poudyal et al., 2014). Nepal boasts a diverse and unique topography, characterized by diverse geographical conditions and varied environments. It is highly influenced by severe exposure to solar UV radiation due to its proximity to the equator. Solar ultraviolet radiation (Holland, 2020; Pondyal et al., 2012) plays a vital role in all ecosystems of living and non-living entities, aquatic animals, and plants, including humans, in the Earth's atmosphere and on its

†Khem N. Poudyal, Babu R. Tiwari and Binod K. Bhattarai contributed equally to this work.

*Correspondence:
Umakant L. Karna
ulkarna5@gmail.com
[1]Department of Physics, Amrit Campus, IOST, TU, Thamel, Kathmandu, Bagmati, Nepal
[2]Central Department of Physics, Tribhuvan University (TU), Kirtipur 44618, Nepal
[3]Department of Applied Sciences and Chemical Engineering, Pulchowk Campus, IOE, TU, Pulchowk, Lalitpur, Bagmati, Nepal

surface through both adverse and advantageous effects when propagated in the atmosphere (Bernhard et al., 2023; Diffey, 2002; Lucas et al., 2019). Research activities have accelerated over the last five decades to study the variability of solar UV radiation using various techniques (Reis et al., 2022). The UV radiation is quantified in terms of the Ultraviolet Index (UVI), a dimensionless quantity that measures UV radiation levels on the Earth's surface (Fioletov et al., 2010; Vitt et al., 2020). It indicates the erythemal (redness in the skin) impacts on the human body, ranging from 0 at night to + 11 at noon in summer near the tropics. The UVI is used to raise public awareness of the adverse effects of UV radiation and alert individuals to the need for sun protection to reduce their risk of skin cancer (World Health Organization et al., 2002; Bhattarai, 2007). Solar UV radiation is affected by geographical parameters, environmental parameters (ozone, aerosols, clouds), surface albedo, and altitude through absorption and scattering processes (Aun et al., 2020; Kerr, 2005; Andrady et al., 2023). The UV Index provides significant information about UV radiation climatology at a location, and data from OMI satellite estimates are compared with NILU UV meter data for validation (Kerr & Fioletov, 2008).

Different mysteries concerning solar UV radiation in atmospheric research have been explored since the discovery of the ozone hole (Farman et al., 1985). The role of solar UV radiation on the development of living organisms and nonliving materials has been explored by measuring various related quantities with numerous approaches (Fountoulakis et al., 2016). Measurements of solar UVR and its products under different atmospheric conditions have been examined using different satellites (TOMS and OMI, etc.) estimates and ground-based instruments, as well as with various simulations and model calculations. The solar UVR and its validation at several historical stations around the world have been used to measure in different countries (dos Reis et al., 2024; Klotz et al., 2025), such as Canada, Europe, the USA, New Zealand, etc., generally at higher latitudes and altitudes (Fountoulakis et al., 2018). Nowadays, very extensive studies are conducted by discovering different facts and methods in all possible areas and conditions worldwide. The ground-based instruments are spectral Broadband, Moderate Band Filter Radiometer (MBFR), and High-resolution spectral measurements. MBFR (NILU UV meter) requires less manpower and hardware costs and is less complex to operate than high-resolution spectral measurements. UVI is measured with the help of the OMI/Aura satellite and ground-based instrument, MBFR (NILU UV meter (Dahlback et al., 2007)) from 2008 to 2012. The comparison is a necessary task to validate the ground-based data from various instruments with the satellite data (McKenzie et al., 2011; Tanskanen et al., 2007). The studies exposed sites affected by absorbing aerosols or trace gases have biases increased by up to 50%. (Fioletov et al., 2004) found that satellite-estimated data was overestimated by 3 to 11%, but showed zero bias at Saturna Island due to much cleaner air. The study by (Ialongo et al., 2008) reported that satellite data are highly biased in polluted regions. (Sharma et al., 2012) reported that OMI satellite data overestimates ground-based measurements before the monsoon by 27.92% to 71.28%. (Janjai et al., 2014) found the overestimation of satellite UVI by 38% to 60.7% for all sky conditions in Thailand. According to (Cadet et al., 2017) satellite data overestimates ground-based instruments ranged from 0 to 45% depending on the site and time of year.

In recent years, more advanced and reliable ground-based instruments have been developed, providing measurements that show closer agreement with satellite estimates. Therefore, a comprehensive study is necessary to address the current alarming situation of UV radiation in the world. A few studies have investigated the variation of surface ozone and solar UV radiation over different parts of Nepal, India, and the surrounding Indian Ocean region (Singh & Singh, 2004; Kunchala et al., 2022). Despite the growing global concern over UV radiation, Nepal has seen limited research in this field, with national-level initiatives remaining notably insufficient. Due to a lack of long-term ground-based data, except for data from the NILU UV meter from Solar Radiation and Aerosol in the Himalaya Region (SAHR) project of IOE Pulchowk, Nepal, it is difficult to compare both ground-based and satellite data to validate them in the present context. However, this study explores the present topics, taking OMI overpass time data and using 15-day moving average trend analysis, and more statistical tools, such as the Pearson correlation coefficient (r), Mean bias, Root Mean square error (RMSE), and Mean Absolute Percentage error (MAPE) are also incorporated. Moreover, the Section 3 is completed through climatology of solar UV index and total ozone column (TOC), Comparison of Ground-Based and Satellite-Derived Solar UV index, and variation of UVI with altitude.

This paper aims to compare the study of analysis on the Ultraviolet Index using OMI Satellite Data and Ground-Based NILLU UV Radiometer Measurements in Nepal. Also, this study underscores the importance of integrating satellite and ground-based data to enhance public safety and awareness of UV radiation risks. Following Sections 1 introduction, 2, 3, 4, 5, and 6 describe the sites and methodology, results and discussion, conclusion, acknowledgments, and references, respectively.

Table 1 Four Ultraviolet Index monitoring sites in Nepal

Sites	Latitude (°N)	Longitude (°E)	Altitude (m)	Instrument ID	Starting Date
Biratnagar	26.45	87.27	72	133	02.02.2009
Pokhara	28.22	83.32	850	137	01.12.2008
Kathmandu	27.72	85.32	1350	136	04.10.2008
Lukla	27.69	86.73	2850	135	05.10.2009

2 Sites and methodology

2.1 Sites and instruments

Table 1 lists the measurement locations, together with their geographic coordinates, elevations, instrument IDs, and the dates that the measurements began. Biratnagar, situated in the southeastern plains land (Terai), is an industrial hub with a low altitude in a subtropical climate. Pokhara, a mountainous site in mid-western region, is a mid-altitude valley characterized by an urban environment, frequent afternoon rainfall in summer, and proximity to lakes and mountains. Kathmandu, the capital city in a bowl-shaped valley, experiences high urban pollution, particularly from aerosols from factories and vehicles, along with dust during winter. Lukla is a mountainous town in northeastern Nepal, surrounded by rugged terrain and alpine forests, it experiences high UV exposure, thin air, and variable weather due to its high altitude and proximity to the Himalayas. These sites (shown in Fig. 1) encompass a range of altitudes and climatic conditions, from tropical to subtropical, reflecting Nepal's diverse geography.

2.2 Ground-based instrument (NILU UV irradiance meter)

The NILU UV Irradiance Meter (shown in Fig. 2), funded by the Development, Research, and Education (NUFU) program in close cooperation with the Norwegian University of Science and Technology (NTNU) from 2007 to 2012, operates under the Solar Radiation and Aerosol in the Himalayan Region (SAHR) project. This UV monitoring program was initiated at the Institute of Engineering, Pulchowk Campus, Tribhuvan University, and maintained four monitoring sites in Nepal from 2008 to 2012. The instrument is manufactured by the Norwegian Institute for Air Research (NILU).

Fig. 2 NILU Irradiance UV meter

It has six channels, five of which are in the UV region with center wavelengths of 305, 312, 320, 340, and 380 nm and a bandwidth of 10 nm at FWHM. The sixth channel measures photosynthetically active radiation, with a bandwidth of 300 nm at FWHM and wavelengths ranging from 400 to 700 nm. Data is recorded in a built-in data logger capable of storing three weeks of 1-minute averages at a one-minute resolution, and the system is stabilized at 50°C. The fully operational instrument weighs 3.3

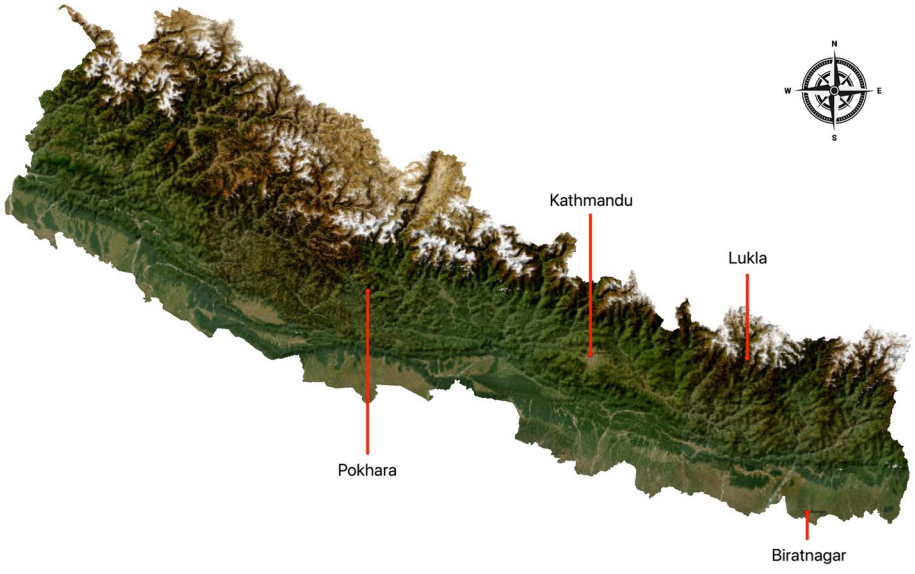

Fig. 1 Map of Nepal showing study sites

kg, is waterproof, and can function under harsh environmental conditions (Høiskar et al., 2003).

2.3 OMI/Satellite

NASA's Earth Observing System (EOS) Aura satellite houses a nadir-viewing near-UV/visible CCD spectrometer called the Ozone Monitoring Instrument (OMI). Since August 9, 2004, OMI has been gathering data from this satellite platform, which was launched in July of that year. It is contributed by the Netherlands's Institute for Air and Space Development (NIVR) of Delft in collaboration with the Finnish Meteorology Institute (FMI), Helsinki, Finland, USA to the EOS Aura mission (Schoeberl et al., 2008). With a spectral resolution of 0.42 nm in the ultraviolet and 0.63 nm in the visible region, the OMI processes solar reflected and backscattered radiation with wavelengths ranging from 264 nm to 504 nm to 500 nm. The normal ground footprint at the nadir is 13 × 24 km^2. It can continuously map the entire world every day and has a viewing swath that is 2600 km wide. It can differentiate between several types of aerosols, including dust, smoke, and sulphates. It can also map the international distribution and trends in UV-B radiation. The equatorial crossing local time of the Aura satellite is 13:42 hours, and its orbital period is around 98 minutes. It can operate in all weather conditions and has worldwide coverage. Here, the analysis of this study is done using the OMI data. For the most recent information about OMI data products, it is recommended to refer to the OMI README files.

2.4 Method and statistical analysis

The solar UV Index and total ozone column during satellite UV overpass time using sources satellite estimates and NILU UV irradiance meter data pairs from each station are collected and refined all the meaningful data with the help of some standard terms like Lambertian Equivalent Reflectivity (LER) at 360 nm available in the OMI overpass data to screen the data into two groups i.e., cloud-free and cloudy. The data with LER greater than 0.1 are cloudy, whereas those with less than 0.1 are cloud-free (Kalliskota et al., 2000). Also, the absent data are filled with average values of data from both ends, i.e., previous and after-gap data. The ground values of UVI are equal to 0.3 is taken as the threshold value since small UVI values are unstable for comparison (Tanskanen et al., 2007). Since the number of cloudy data points is found to be very small so it is not removed, and the study continues with all data under all-sky conditions, assuming a minor change in results. The scatter plots between satellite OMI and ground-based data are plotted to analyze different sites and atmospheric conditions. The cloud-free data are used for comparison to filter or minimize the errors due to clouds, as they add maximum errors. Then, the Pearson correlation coefficient (r), Mean bias, Root Mean square error (RMSE), and Mean Absolute Percentage error (MAPE) are calculated and analyzed using the following formulas.

To facilitate a valid intercomparison between satellite and ground-based UV measurements, an organized data processing workflow was followed. Data processing was structured into three phases: satellite data processing, ground-based data processing, and integration of data. In each phase, data quality, temporality, and intercomparison were preserved between both measurement systems.

i. *Satellite Data Processing* Files of UV measurements from OMI/AURA Level-2 products were downloaded directly from the NASA Goddard Earth Sciences Data and Information Services Center (GES DISC).
ii. For quality assurance of the data, anomalies in the cloud-screened UV index (CSUVindex) were detected by the Isolation Forest algorithm (contamination = 0.01). The flagged outlier observations were not discarded but imputed instead by a K-Nearest Neighbors (KNN) regression model.
The KNN regression approach was selected for being non-parametric and for its ability to consider local, nonlinear relationships without the need for a functional form. This maintains corrected values consistent with neighboring valid observations.
The predictor variable for KNN was the distance between the observation station and the OMI Cross Track Position (0–59). Since satellite-derived UV measurements are largely a function of geometric configuration, this distance provides a physically meaningful feature to predict corrected CSUVindex values.
iii. *Ground-Based Data Processing* Ground-based spectral UV data were obtained from NILU-UV multi-channel radiometers placed at Biratnagar, Kathmandu, Lukla, and Pokhara. Because NILU instruments were measured at minute-level time resolution, but OMI overpass data were available only once per day, the NILU dataset was downsampled to overpass times. For each satellite overpass, the nearest NILU measurement in time was taken, creating temporal agreement between the two datasets. The NILU dose rate measurements were then converted to a ground-based UV index (GDUVindex) by multiplying it by 40 (Sola et al., 2008).
iv. *Data Integration* Satellite and ground-based data were merged on the OMI overpass time for each station. The resulting data contained satellite-derived parameters with ground-based NILU

measurements. The merged dataset included temporally and spatially collocated OMI and NILU instrument UV index values. It enabled stable comparison of satellite retrievals and ground-based observations under identical observation conditions by enabling anomaly correction, calibration, and time alignment.

Several statistical metrics were employed to examine agreement and performance among satellite-retrieved and ground UV index values. These metrics evaluate different aspects of accuracy, bias, and variability in the comparison, yielding an integrated picture of the datasets.

i. Pearson correlation coefficient (r):

$$\frac{\sum_{i=1}^{N}(UVI_S - \overline{UVI_S})(UVI_G - \overline{UVI_G})}{\sqrt{\sum_{i=1}^{N}(UVI_S - \overline{UVI_S})^2 \sum_{i=1}^{N}(UVI_G - \overline{UVI_G})^2}}$$

Where UVI_S, UVI_G, $\overline{UVI_S}$ and $\overline{UVI_G}$ are the satellite, ground-based, and their respective average values, and N is the number of observations.

ii. Mean bias:

$$\frac{1}{N}\sum_{i=1}^{N}(UVI_S - UVI_G)$$

iii. Relative bias:

$$\frac{\sum_{i=1}^{N}(UVI_S - UVI_G)}{\sum_{i=1}^{N} UVI_G} \times 100\%$$

Where UVI_S and UVI_G are the satellite and ground-based values of UVI, respectively, and N is the number of observations.

iv. Root mean square error (RMSE):

$$\sqrt{\frac{\sum_{i=1}^{N}(UVI_S - UVI_G)^2}{N}}$$

Where UVI_S and UVI_G are the satellite and ground-based values of UVI *respectively, and N is the number of observations.*

v. Mean absolute percentage error (MAPE):

$$\frac{1}{N}\sum_{i=1}^{N}\left|\frac{UVI_S - UVI_G}{UVI_G}\right|$$

Where UVI_S, UVI_G, and N are the satellite, ground-based values of UVI and the number of observations, respectively (Mohamed et al., 2023).

3 Results and discussion

This section is completed with the help of Climatology of Solar UV Index and total ozone column (TOC), comparisons of UV index, Comparison of Ground-Based and Satellite-Derived Solar UV Index, and Variation of UVI with altitude in the following subsections.

3.1 Climatology of solar UV index and total ozone column (TOC)

The box plot for the ground-based UV index and TOC at four locations under all-sky conditions from 2008 to 2012 is displayed in Fig. 3a. The maximum UV Index values for Biratnagar, Pokhara, Kathmandu, and Lukla are 10.6, 15.4, 14.5, and 17.4, respectively, while the median UV Index values are 6.0, 7.5, 6.2, and 9.5, as shown in Fig. 3a. It is similar to other countries, India, and Thailand, (Bhattacharya et al., 2012; Janjai et al., 2014; Kunchala et al., 2022). It is attributed to generally higher UV levels at lower latitudes and higher altitudes due to variations in atmospheric loading of aerosols and cloud cover. Also, during OMI overpass times, the sun's higher position in the sky at lower latitudes enhances UV exposure due to the more direct solar angle. Fig. 3b presents the box plot of the ground-based total ozone column (TOC) at these sites during the same period. The median TOC values are 270 DU, 265 DU, 265 DU, and 260 DU, while the maximum TOC values are 310 DU, 308 DU, 307 DU, and 300 DU for Biratnagar, Pokhara, Kathmandu, and Lukla, respectively. The level of solar UV index increases as the altitude of the site rises, except in Kathmandu, as discussed above. However, the value of TOC decreases at corresponding sites as shown in Fig. 3b, supporting the inverse relationship between UV index and TOC. The value of TOC lies between (275–300) DU in Pakistan and northern India, close to Nepal, which lies between (264–270) DU and similar to other countries, depending on altitude, sites, and time (Kunchala et al., 2022; Rafiq et al., 2017; Resmi et al., 2021).

Figure 4 illustrates the relative frequency distribution of UVI exposure categories (as defined in Table 2) with corresponding color codes. According to World Health Organization et al. (2002), UVI exposure is categorized into five classes: low, moderate, high, very high, and extreme, with color coding. The UVI distribution in Lukla is predominantly characterized by "High," "Very High," and "Extreme" values, which collectively account for over 80% of the total observations from March to September. The "Moderate" and "High" categories are more prevalent in winter. The UVI levels decrease progressively from

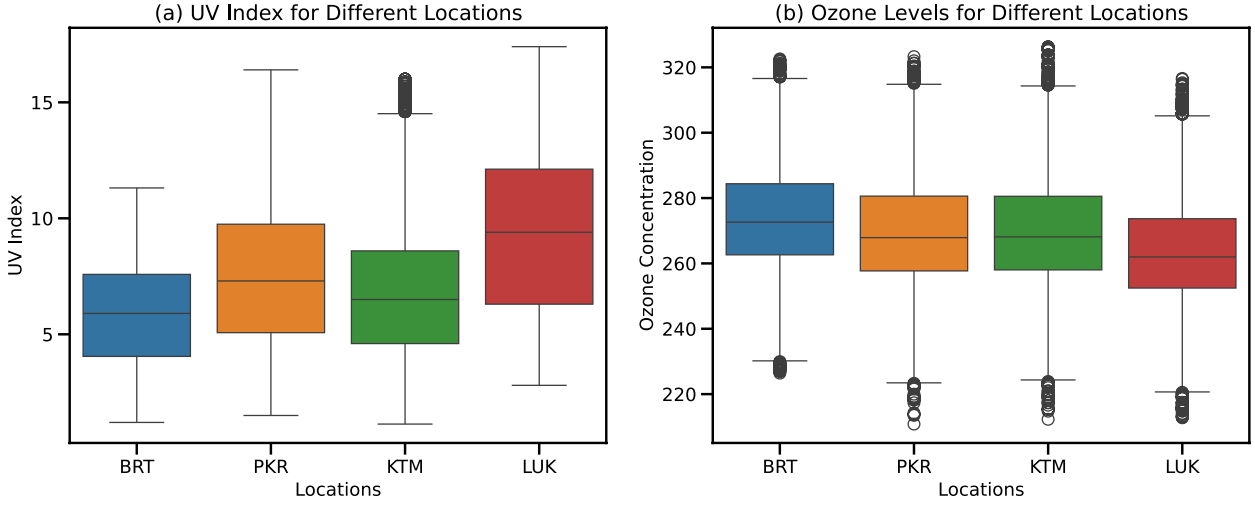

Fig. 3 Box plot of overpass UVI (**a**) and TOC (**b**) using ground-based measurement data at Kathmandu, Biratnagar, Pokhara, Kathmandu, and Lukla. *BRT* stands for Biratnagar, *PKR* stands for Pokhara, *KTM* stands for Kathmandu, and *LUK* stands for Lukla

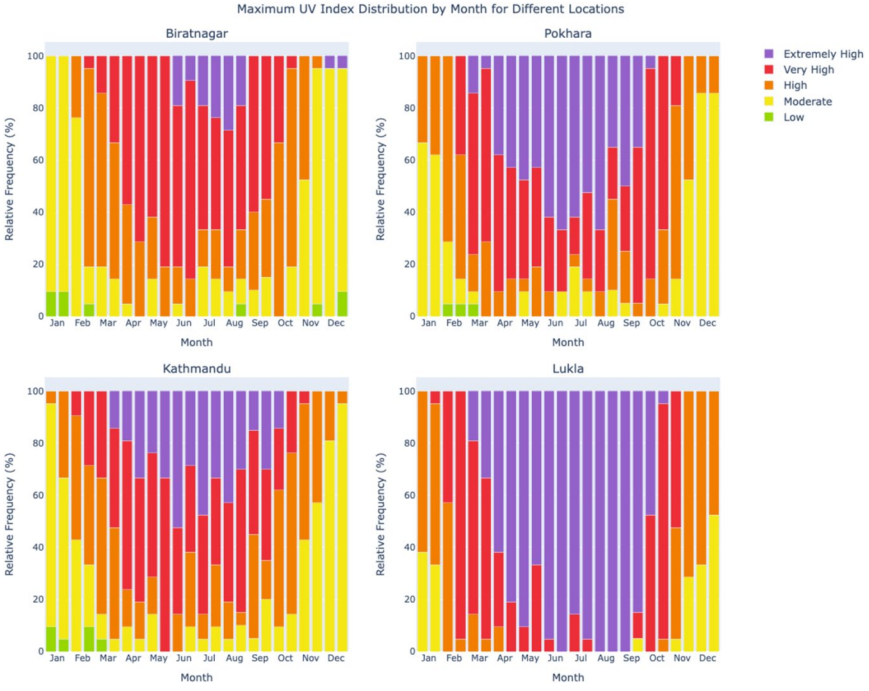

Fig. 4 Relative frequency of UVI exposure categories along with color code

Table 2 UVI Exposure categories for WHO Standard

SN	Exposure categories	UVI
1	Low	1 to 2
2	Moderate	3 to 5
3	High	6 to 7
4	Very High	8 to 10
5	Extremely High	11+

The *UNEP* United Nations Environment Program, the *WHO*World Health Organization,the *WMO* World Meteorological Organization, and the *ICNIRP* International Commission on Non-Ionizing Radiation Protection have jointly recommended UVI exposure categories

Lukla to Pokhara, Kathmandu, and are lowest in Biratnagar, along with their respective site exposure categories shown in Fig. 4 and Table 2. Therefore, Lukla is badly influenced by exposure to solar UV radiation and hence needs to take necessary precautions while moving in this region. The government of Nepal is advised to prioritize forecasting UV index values alongside other meteorological parameters. This would be particularly significant for mid-hill and high-altitude regions, where UV exposure is more intense. Implementing such a system would greatly improve the safety of trekkers, tourists, and locals in the

high mountains, reducing the risk of adverse effects from UV radiation.

3.2 Comparison of ground-based and satellite-derived solar UV index

Figure 5 compares the daily changes in the UV Index between two datasets with OMI estimates and ground-based measurements data with the help of trend analysis of OMI overpass UVI, and NILU UVI data with 15 day moving averages and found that the UV index has seasonal variations with higher UV index values in summer (June-August) and lower values in winter (December-February) in all sites. Although the trends of satellite and ground-based measurements are similar, OMI UVI consistently overestimates ground-based UVI, aligning with global findings. Here, the dark blue and green curves represent the 15-day moving average, whereas the light blue and green curves give the standard deviation for satellite and ground-based data, respectively.

Here, the dark blue and green curves represent the 15-day moving average, whereas the light blue and green curves represent the standard deviation for satellite and ground-based data, respectively. The OMI satellite's moving average curve is smoother than ground-based data at all sites, reflecting the satellite's simplicity compared to the complex, UVI-affecting factors influencing ground measurements.

The OMI Satellite has a wide field of view, and the average value of UVI in this region represents the local UVI, whereas ground-based instruments capture the UVI at a point or at a very small region affected by local factors, resulting in more fluctuations on the ground-based instrument (NILU). The fluctuations in standard deviation are also higher in ground-based data relative to satellite estimates during spring and summer(maximum), except in the winter season. The rise of aerosols after winter causes fluctuations in UVI on the ground in spring but gives maximum deviations in summer due to clouds, whereas least aerosol and clouds(nearly clean atmosphere) in winter, giving the least fluctuations. The satellite and ground data with their respective moving averages and standard deviations in Biratnagar are distinctly separated from the rest of the sites. This is because the topography, environmental factors, and other factors in Biratnagar have a simple pattern, even in winter, compared to mountainous sites. Kathmandu is highly affected by pollution emitted from vehicles, factories, brick kilns, etc, and sometimes, albedo due to snow present in the nearby mountains in winter, cup-shaped valley topography, boundary layer aerosols, and clouds that provide its climatology (Poudyal et al., 2014; Sharma et al., 2011). Pokhara and Lukla are affected by the complex nearby Himalayas, which have winter snow and heavy rains in summer (in Pokhara). Despite these local factors, the algorithms of OMI satellites may not be able to resolve exactly the polluted layers of the lower atmosphere of urban areas (Janjai et al., 2014). The assumption of clouds as a plane-parallel medium (Tanskanen et al., 2007) adds some measurement errors under cloudy conditions due to observed deviations from ground-based

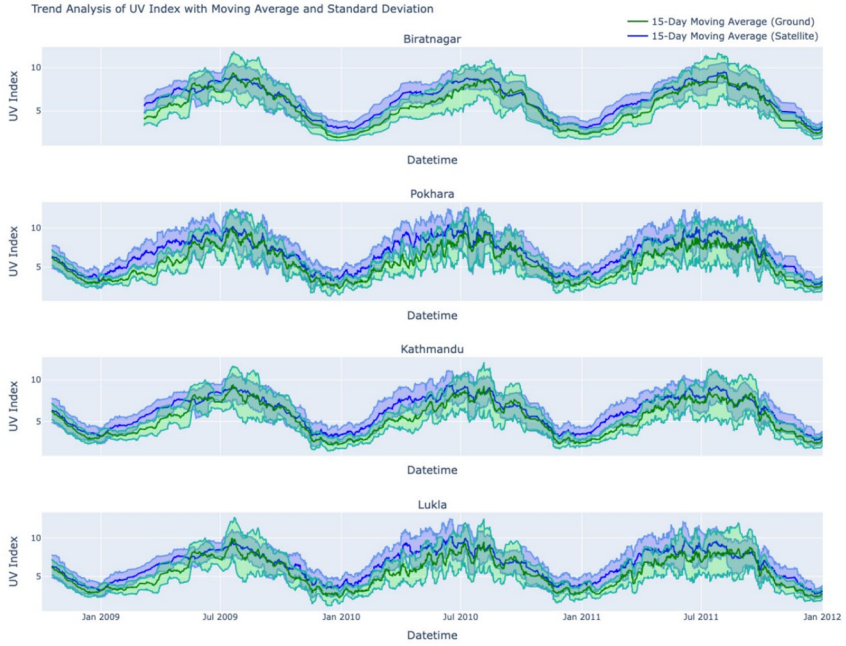

Fig. 5 Trend analysis of OMI overpass UVI, and NILLU data with the moving average during the period 2008-2012. The dark blue and green curves represent the 15-day moving average, while the light blue and green curves indicate the standard deviation for satellite and ground-based data, respectively

measurements. Also, the satellite's algorithm could not distinguish the presence of clouds and snow, a complex condition which is another important factor in the increase of errors. The mismatch of time and space resolutions between the satellite and ground-based measurements also adds to the error from the variability of clouds (Ialongo et al., 2008). In winter, it is seen that there is the least (somewhere a negative value) minimum UVI at Pokhara and Lukla compared to Kathmandu and Biratnagar due to their pristine environmental conditions. These discussed factors for different sites provide an idea for comparisons of UVI from both datasets.

The scatter plot in Fig. 6 compares OMI overpass coincident UV index values with ground-based UV measurements at all four sites under all-sky conditions. In this plot, the ground-based data are plotted along the x-axis and the OMI data along the y-axis, enabling an assessment of the correlation between the two datasets. The solid black diagonal line is the bisectrix of a 1:1 ratio, and the red broken line is the regression fit line for all-sky data. Fig. 6 shows that the OMI satellite data yield higher UV index values than the ground-based measurements, with the regression line equation, coefficient of determination (R^2), and correlation coefficient for each site also presented. The satellite estimates UVI mean(μ), ground-based UVI mean data (μ), and their mean bias, relative bias (%), mean absolute percentage error (MAPE) (%), root mean square error (RMSE), correlation coefficient (r), and standard deviation of bias(σ) are shown in Table 3. The least relative bias and correlation coefficient for summer compared to the rest of the seasons indicates that there is strong agreement but poor alignment between the two datasets in this season due to the washing out of the atmosphere with rain. Table 3 shows that autumn has a greater mean bias, relative bias, RMSE, and MAPE than summer, while the correlation coefficients are highest (0.8) in both autumn and winter. This indicates that the datasets are strongly aligned and well-matched in these seasons, with the smallest deviations in autumn and winter (occasional large deviations). The reduced errors in autumn are likely due to predominantly clear-sky conditions, as aerosol and cloud amounts are at their lowest extent, which increases in winter. The high RMSE values in spring and summer mean a large average magnitude of difference in errors in comparison to other seasons, as shown in Fig. 5 and Table 3.

During the summer, Pokhara records the highest UV Index among all sites across all seasons. This is attributed

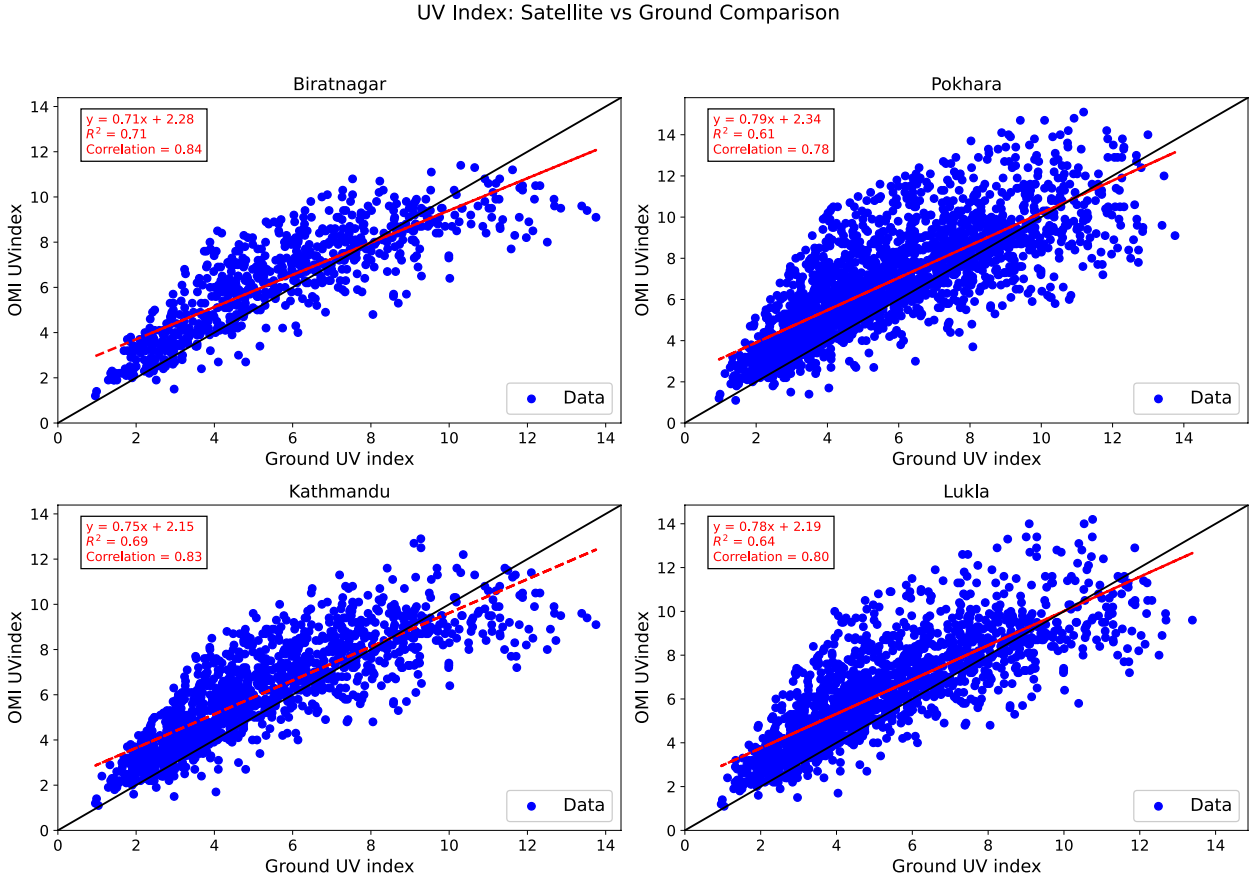

Fig. 6 Scatter plot for Comparison of OMI overpass UV index with ground-based UV index at Biratnagar, Pokhara, Kathmandu, and Lukla

Table 3 Descriptive statistics of UV index comparison for satellite data and ground-based data for all-sky conditions

Location	Season	Ground Data Mean(μ)	Satellite Data Mean(μ)	Mean Bias	Relative Bias (%)	MAPE (%)	RMSE	Correlation Coefficient (r)
Biratnagar	Winter	3.08	4.11	1.04	33.65	37.09	1.33	0.78
	Spring	6.03	7.36	1.33	22.09	31.36	1.96	0.62
	Summer	7.88	8.36	0.48	6.05	24.99	1.97	0.6
	Autumn	4.9	5.37	0.47	9.58	22.88	1.28	0.82
Pokhara	Winter	3.27	4.42	1.15	35.09	38.56	1.43	0.8
	Spring	6.21	8.12	1.92	30.9	42.32	2.65	0.57
	Summer	8.12	9.02	0.9	11.14	30.75	2.53	0.49
	Autumn	5.15	5.84	0.69	13.47	27.49	1.67	0.75
Kathmandu	Winter	3.25	4.32	1.08	33.14	37.24	1.37	0.8
	Spring	6.27	7.83	1.56	24.9	35.72	2.26	0.65
	Summer	7.84	8.6	0.77	9.76	30.79	2.38	0.5
	Autumn	4.84	5.47	0.62	12.84	25.91	1.44	0.77
Lukla	Winter	2.89	3.82	0.93	32.1	36.22	1.16	0.83
	Spring	6	7.01	1.01	16.89	26.92	1.62	0.67
	Summer	7.99	8.39	0.4	5.03	22.82	1.93	0.54
	Autumn	5.15	5.44	0.29	5.61	20.24	1.19	0.85

Statistics of UV index comparison for satellite data and ground-based data for all-sky conditions

to rainfall, which clears the atmosphere, allowing more UV radiation to reach the surface. Kathmandu would typically have a higher UV Index than Pokhara due to the solar altitude effect, but this is not observed. The lower UV Index in Kathmandu is likely due to high aerosols caused by pollution from vehicles, factories, brick kilns, and other sources, combined with the effects of the boundary layer. It is also attributed to snow in the nearby Himalayas at Pokhara. Conversely, occasional cloud cover in Pokhara may contribute to a slight decrease in its UV Index compared to Kathmandu under certain conditions. Table 3 also indicates that the maximum bias initially observed in Pokhara gradually diminishes as it moves through Kathmandu and Biratnagar, before reaching its lowest value in Lukla. The bias exhibits a seasonal pattern, starting at its highest in spring, gradually decreasing through winter and summer, and peaking again in autumn. The bias is due to the aerosol and cloud in the atmosphere over respective sites and seasons.

As the temperature rises, the atmosphere is loaded with variable amounts of aerosol from continental and non-continental sources from the Bay of India and Bengal. The albedo effect from the nearby Himalayan region, like Annapurna, may enhance solar UV irradiance in Pokhara, potentially contributing to measurement biases. The relative bias (%) is in decreasing order starting from

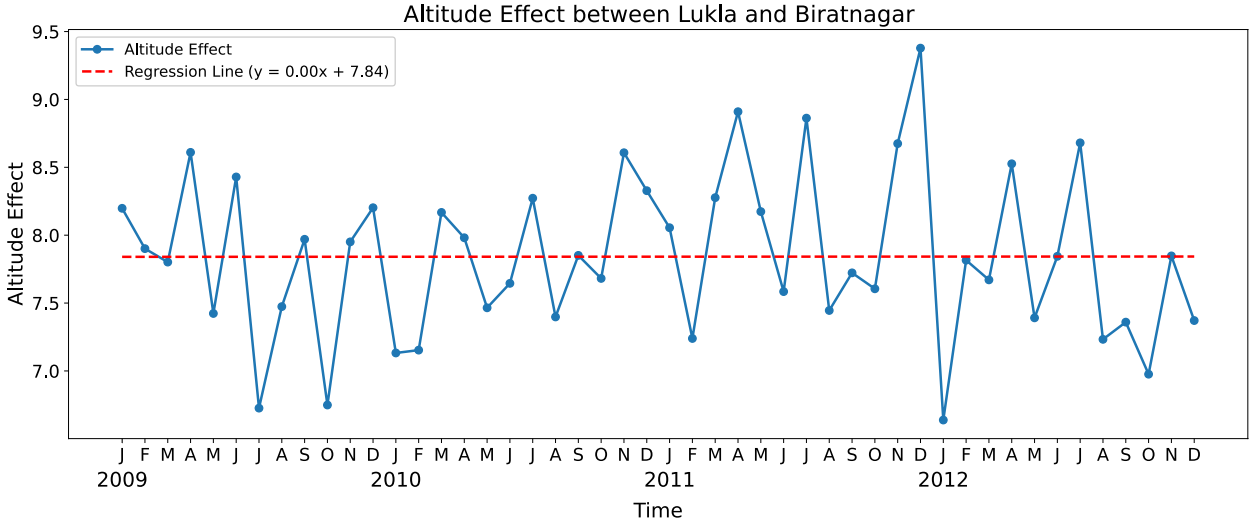

Fig. 7 Altitude effect between Lukla and Biratnagar

winter to Spring, autumn, and minimum at summer. However, the correlation coefficient(r) has a maximum value in autumn, then in winter, spring, and a minimum in summer.

3.3 Variation of UVI with altitude

The solar UVR increases with the rise in altitude above sea level. The variations of solar UVI for Biratnagar, Kathmandu, Pokhara, and Lukla are shown in Figs. 3 and 4. The increasing solar UV radiation flux with respect to height is called the altitude effect (Sola et al., 2008). Its unit is %/Km. It is due to the decreasing amount of air molecules, aerosols, ozone, clouds, covered and snow-covered surfaces, and clean air. The Altitude effects (AE) depend on factors such as the wavelength of the radiation, the solar zenith angle, the amount of air mass, and turbidity. Fig. 7 shows the altitude effects for Lukla and Biratnagar that range (6.5–8.8.5.8) %/Km. During winter, large peaks were observed, which may be due to a large significant albedo effect at Lukla.

4 Conclusions

The study compared the satellite UVI estimates data with ground-based measured data at Biratnagar, Pokhara, Kathmandu, and Lukla stationed in different environmental and geographical conditions in Nepal. It is aimed to evaluate the accuracy of satellite-based UV index and TOC relative to ground-based measurements and find a measurable bias when compared to ground-based measurements. The analysis revealed that satellite data generally overestimated UVI values but underestimated TOC values compared to ground-based data, with a mean bias, relative bias, and correlation coefficient ranges from 0.29 to 1.92, from 5.03% to 33.65%, and from 0.5 to 0.85 for UVI, respectively. Likewise, a mean bias, relative bias, and correlation coefficient range from −14.87 to 1.96, −4,96% to 0.6%, and 0.73 to 0.94 for TOC, respectively. Other statistical tools such as MAPE, RMSE, and the standard of bias of UVI or TOC, suggest a strong linear relationship between the two datasets and highlight the potential for further refinement of satellite algorithms to improve accuracy. The result also shows that the altitude effect is approximately (6.5–8.8.5.8)%/km. Despite the limited geographical scope of the study, these findings offer important insights for enhancing UV radiation monitoring systems. Future research should focus on expanding ground-based data networks and refining satellite models to serve as public health initiatives. Similarly, the variability and trends of the UV index in Nepal will be studied in the future.

Acknowledgements

The authors would like to thank NASA/USA for providing the Ozone Monitoring Instrument (OMI) data on the Ultraviolet (UV) Index, which was crucial to the success of this study. It is also a great pleasure to thank the Solar Radiation and Aerosols Project in the Himalayan Region, Institute of Engineering, Pulchowk, for providing the NILU UVI data.

Authors' contributions

Umakant L. Karna: Conceptualization, data analysis, manuscript preparation, and overall coordination. Khem N. Poudyal: Literature review, error analysis, and data validation. Babu R. Tiwari: Software implementation, testing, and validation of results. Binod K. Bhattarai: Supervision, critical review, and overall corrections.

Funding

No financial support was received for this research.

Data availability

The OMI satellite data were obtained from the Atmospheric Composition Validation Data Center (AVDC), a centralized, long-term archive for validation datasets maintained by the Atmospheric Chemistry and Dynamics Branch at NASA's Goddard Space Flight Center (GSFC), Greenbelt, Maryland https://avdc.gsfc.nasa.gov/. Ground-based data were obtained from NILU irradiance meters installed at the selected sites. Upon request, the corresponding author will provide the data used to construct the figures and tables.

Declarations

Competing interests

The authors have no recognized competing interests.

Received: 12 May 2025 / Accepted: 11 November 2025
Published online: 17 December 2025

References

Adhikari, K. R., Bhattarai, B. K., & Gurung, S. (2013). Estimation of global solar radiation for four selected sites in Nepal using sunshine hours, temperature and relative humidity. *Journal of Power and Energy Engineering,01*(03), 1–9.

Andrady, A. L., Heikkilä, A. M., Pandey, K. K., Bruckman, L. S., White, C. C., Zhu, M., & Zhu, L. (2023). Effects of UV radiation on natural and synthetic materials. *Photochemical & Photobiological Sciences,22*(5), 1177–1202.

Aun, M., Lakkala, K., Sanchez, R., Asmi, E., Nollas, F., Meinander, O., Sogacheva, L., De Bock, V., Arola, A., de Leeuw, G., Aaltonen, V., Bolsée, D., Cizkova, K., Mangold, A., Metelka, L., Jakobson, E., Svendby, T., Gillotay, D., & Van Opstal, B. (2020). Solar UV radiation measurements in Marambio, Antarctica, during years 2017–2019. *Atmospheric Chemistry and Physics,20*(10), 6037–6054.

Bernhard, G. H., Bais, A. F., Aucamp, P. J., Klekociuk, A. R., Liley, J. B., & McKenzie, R. L. (2023). Stratospheric ozone, UV radiation, and climate interactions. *Photochemical & Photobiological Sciences,22*(5), 937–989.

Bhattacharya, R., Pal, S., Bhoumick, A., & Barman, P. (2012). Annual variability and distribution of ultraviolet index over India using Temis data. *International Journal of Engineering Science and Technology*, 4:4577

Bhattarai, B. K. (2007). Factors affecting solar ultraviolet radiation, based on some case studies in Norway and Nepal. Doctoral thesis, Norwegian University of Science and Technology (NTNU). (pp. 26–27).

Cadet, J.-M., Bencherif, H., Portafaix, T., Lamy, K., Ncongwane, K., Coetzee, G., & Wright, C. (2017). Comparison of ground-based and satellite-derived solar UV index levels at six South African sites. *International Journal of Environmental Research and Public Health,14*(11), 1384.

Dahlback, A., Gelsor, N., Stamnes, J. J., & Gjessing, Y. (2007). UV measurements in the 3000–5000 m altitude region in Tibet. *Journal of Geophysical Research*. https://doi.org/10.1029/2006JD007700

Diffey, B. L. (2002). Sources and measurement of ultraviolet radiation. *Methods,28*(1), 4–13.

dos Reis, G. C. G., Bencherif, H., Silva, R., Vaz Peres, L., dos Reis, M. A. G., Pinheiro, D. K., da Silva, F. R., Lamy, K., & Portafaix, T. (2024). Comparative analysis of ground-based and satellite-derived UV index levels in Natal, Brazil. *Remote Sensing,16*(24), Article 4687.

Farman, J. C., Gardiner, B. G., & Shanklin, J. D. (1985). Large losses of total ozone in Antarctica reveal seasonal ClOx/NOx interaction. *Nature,315*(6016), 207–210.

Fioletov, V., Kerr, J. B., & Fergusson, A. (2010). The UV index: Definition, distribution and factors affecting it. *Canadian Journal of Public Health,101*(4), I5-9.

Fioletov, V. E., Kimlin, M. G., Krotkov, N., McArthur, L. J. B., Kerr, J. B., Wardle, D. I., Herman, J. R., Meltzer, R., Mathews, T. W., & Kaurola, J. (2004). UV index climatology over the United States and Canada from ground-based and satellite estimates. *Journal of Geophysical Research*. https://doi.org/10.1029/2004JD004820

Fountoulakis, I., Bais, A. F., Fragkos, K., Meleti, C., Tourpali, K., & Zempila, M. M. (2016). Short- and long-term variability of spectral solar UV irradiance at Thessaloniki, Greece: Effects of changes in aerosols, total ozone and clouds. *Atmospheric Chemistry and Physics,16*(4), 2493–2505.

Fountoulakis, I., Zerefos, C. S., Bais, A. F., Kapsomenakis, J., Koukouli, M.-E., Ohkawara, N., Fioletov, V., De Backer, H., Lakkala, K., Karppinen, T., & Webb, A. R. (2018). Twenty-five years of spectral UV-B measurements over Canada, Europe and Japan: Trends and effects from changes in ozone, aerosols, clouds, and surface reflectivity. *Comptes Rendus Geoscience,350*(7), 393–402.

Høiskar, B. A. K., Haugen, R., Danielsen, T., Kylling, A., Edvardsen, K., Dahlback, A., Johnsen, B., Blumthaler, M., & Schreder, J. (2003). Multichannel moderate-bandwidth filter instrument for measurement of the ozone-column amount, cloud transmittance, and ultraviolet dose rates. *Applied Optics,42*(18), 3472–3479.

Holland, J. (2020). Reproduction without polarity in the work of Johann Wilhelm Ritter. *History and Philosophy of the Life Sciences,42*(4), 52.

Ialongo, I., Casale, G. R., & Siani, A. M. (2008). Comparison of total ozone and erythemal UV data from OMI with ground-based measurements at Rome station. *Atmospheric Chemistry and Physics,8*(12), 3283–3289.

Janjai, S., Wisitsirikun, S., Buntoung, S., Pattarapanitchai, S., Wattan, R., Masiri, I., & Bhattarai, B. K. (2014). Comparison of UV index from ozone monitoring instrument (OMI) with multi-channel filter radiometers at four sites in the tropics: Effects of aerosols and clouds. *International Journal of Climatology,34*(2), 453–461.

Kalliskota, S., Kaurola, J., Taalas, P., Herman, J. R., Celarier, E. A., & Krotkov, N. A. (2000). Comparison of daily UV doses estimated from nimbus 7/TOMS measurements and ground-based spectroradiometric data. *Journal of Geophysical Research,105*(D4), 5059–5067.

Kerr, J. B. (2005). Understanding the factors that affect surface ultraviolet radiation. *Optical Engineering,44*(4), 041002.

Kerr, J. B., & Fioletov, V. E. (2008). Surface ultraviolet radiation. *Atmosphere-Ocean,46*(1), 159–184.

Klotz, B., Gradl, R., Schenzinger, V., Schwarzmann, M., Schreder, J., Lorenz, S., Gröbner, J., Hülsen, G., & Kreuter, A. (2025). UV map nowcasting and comparison with ground-based UV measurements for the DACH region. *Remote Sensing (Basel),17*(4), 629.

Kunchala, R. K., Singh, B. B., Karumuri, R. K., Attada, R., Seelanki, V., & Kumar, K. N. (2022). Understanding the spatiotemporal variability and trends of surface ozone over India. *Environmental Science and Pollution Research,29*(4), 6219–6236.

Lucas, R. M., Yazar, S., Young, A. R., Norval, M., de Gruijl, F. R., Takizawa, Y., Rhodes, L. E., Sinclair, C. A., & Neale, R. E. (2019). Human health in relation to exposure to solar ultraviolet radiation under changing stratospheric ozone and climate. *Photochemical & Photobiological Sciences,18*(3), 641–680.

McKenzie, R. L., Aucamp, P. J., Bais, A. F., Björn, L. O., Ilyas, M., & Madronich, S. (2011). Ozone depletion and climate change: Impacts on UV radiation. *Photochemical & Photobiological Sciences,10*(2), 182–198.

Mohamed, M. S., Abdel Wahab, M. M., El-Metwally, M., & El-Nobi, E. F. (2023). Validation of UV-Index retrieved from three satellites against Ground-Based measurements at different climates in Egypt. *The Egyptian Journal of Remote Sensing and Space Sciences,26*(2), 361–367.

Pondyal, K. N., Bhattarai, B. K., Sapkota, B., & Kjeldstad, B. (2012). Solar radiation potential at four sites of Nepal. *Journal of The Institution of Engineers,8*(3), 189–197.

Poudyal, K. N., Bhattarai, B. K., Sapkota, B. K., Kjeldstad, B., & Karki, N. R. (2014). Estimation of global solar radiation using pyranometer and NILU-UV irradiance meter at Pokhara valley in Nepal. *Journal of the Institute of Engineering,9*(1), 69–78.

Rafiq, L., Tajbar, S., & Manzoor, S. (2017). Long term temporal trends and spatial distribution of total ozone over Pakistan. *The Egyptian Journal of Remote Sensing and Space Sciences,20*(2), 295–301.

Reis, G., Souza, S., Neto, H., Branches, R., Silva, R., Peres, L., Pinheiro, D., Lamy, K., Bencherif, H., & Portafaix, T. (2022). Solar ultraviolet radiation temporal variability analysis from 2-year of continuous observation in an Amazonian city of Brazil. *Atmosphere,13*(7), Article 1054.

Resmi, C. T., Nishanth, T., Vijoy, P. S., Kumar, M. K. S., & Balachandramohan, M. (2021). Analysis of long term variation of the total column and tropospheric ozone over the Indian region. *Atmospheric and Climate Sciences,11*(01), 194–213.

Schoeberl, M. R., Douglass, A. R., & Joiner, J. (2008). Introduction to special section on aura validation. *Journal of Geophysical Research*. https://doi.org/10.1029/2007JD009602

Sharma, N. P., Bhattarai, B. K., Sapkota, B., & Kjeldstad, B. (2012). Comparison of ground based measurements of solar UV index with satellite estimation at four sites of Nepal. *Journal of the Institute of Engineering,8*(3), 58–71.

Sharma, R. R., Kjeldstad, B., & Bhattarai, B. K. (2011). Comparison of UV index and total ozone column of Aura/OMI and ground measurement from Nepal Himalayas. *Journal of the Institute of Engineering,8*(3), 114–129.

Singh, S., & Singh, R. (2004). High-altitude clear-sky direct solar ultraviolet irradiance at leh and hanle in the Western Himalayas: Observations and model calculations. *Journal of Geophysical Research*. https://doi.org/10.1029/2004JD004854

Sola, Y., Lorente, J., Campmany, E., de Cabo, X., Bech, J., Redaño, A., Martínez-Lozano, J. A., Utrillas, M. P., Alados-Arboledas, L., Olmo, F. J., Díaz, J. P., Expósito, F. J., Cachorro, V., Sorribas, M., Labajo, A., Vilaplana, J. M., Silva, A. M., & Badosa, J. (2008). Altitude effect in UV radiation during the evaluation of the effects of elevation and aerosols on the ultraviolet radiation 2002 (VELETA-2002) field campaign. *Journal of Geophysical Research*. https://doi.org/10.1029/2007JD009742

Tanskanen, A., Lindfors, A., Määttä, A., Krotkov, N., Herman, J., Kaurola, J., Koskela, T., Lakkala, K., Fioletov, V., Bernhard, G., McKenzie, R., Kondo, Y., O'Neill, M., Slaper, H., den Outer, P., Bais, A. F., & Tamminen, J. (2007). Validation of daily erythemal doses from ozone monitoring instrument with ground-based UV measurement data. *Journal of Geophysical Research*, *112*(D24).

Vitt, R., Laschewski, G., Bais, A., Diémoz, H., Fountoulakis, I., Siani, A.-M., & Matzarakis, A. (2020). UV-index climatology for Europe based on satellite data. *Atmosphere,11*(7), Article 727.

World Health Organization, World Meteorological Organization, United Nations Environment Programme, and International Commission on Non-Ionizing Radiation Protection (2002). Global solar uv index: A practical guide. WHO/SDE/OEH/02.2. https://iris.who.int/server/api/core/bitstreams/94a908ec-14ee-4bb4-84eb-ace483c9eb51/content

Publisher's Note